

Phase amplification via synthetic two-axis-twisting echo from interaction-fixed one-axis twistingJihao Ma ^{1,2}, Jungeng Zhou ^{1,2}, Jiahao Huang ^{1,2,*} and Chaohong Lee ^{2,3,†}¹*Laboratory of Quantum Engineering and Quantum Metrology, School of Physics and Astronomy, Sun Yat-Sen University (Zhuhai Campus), Zhuhai 519082, China*²*Institute of Quantum Precision Measurement, State Key Laboratory of Radio Frequency Heterogeneous Integration, College of Physics and Optoelectronic Engineering, Shenzhen University, Shenzhen 518060, China*³*Quantum Science Center of Guangdong-Hong Kong-Macao Greater Bay Area (Guangdong), Shenzhen 518045, China*

(Received 17 April 2024; accepted 17 July 2024; published 5 August 2024)

One-axis twisting (OAT) and two-axis twisting (TAT) are well-known methods for achieving entanglement-enhanced quantum metrology, and their time-reversal echo offers a potent tool for approaching the Heisenberg limit even with detection noise. However, flipping the sign of interaction to implement the time-reversal echo is generally challenging. Here, we propose an echo protocol based on synthetic TAT from interaction-fixed OAT in a pseudospin-1/2 ensemble to achieve time-reversal quantum metrology. By applying modulation pulses around two different orthogonal directions, the effective TAT and its echo can be realized without changing the interaction. We demonstrate that this protocol not only outperforms the OAT echo scheme in both metrological gain and evolution time but is also robust against detection noise. Our protocol presents a TAT echo scheme that effectively avoids flipping the sign of interaction, providing a viable method for improving precision and robustness of quantum metrology.

DOI: [10.1103/PhysRevA.110.022407](https://doi.org/10.1103/PhysRevA.110.022407)**I. INTRODUCTION**

The aim of quantum metrology is to use quantum resources such as correlations and entanglement to surpass the classical precision limit [1–4]. It is well known that when using nonentangled states, the phase estimation uncertainty is constrained by the standard quantum limit (SQL), $\Delta\phi_{\text{SQL}} = (\nu N)^{-1/2}$, where ν is the number of identical experiments and N denotes the particle number. The ultimate goal of quantum metrology is to utilize entanglement to reach the Heisenberg limit (HL), $\Delta\phi_{\text{HL}} = \nu^{-1/2} N^{-1}$ [5–8].

One-axis twisting (OAT) [9] has been proposed to generate spin squeezed states [10–12] to outreach the SQL. Up to date, many proof-of-principle experiments have been demonstrated with various systems such as atomic Bose-Einstein condensates (BECs) [13–15], trapped ions [16], and cold atoms in an optical cavity [17,18]. However, using the spin squeezed states generated by OAT, the phase estimation uncertainty is only proportional to $N^{-5/6}$, and the optimal squeezing angle depends on the particle number N and the evolution time T [5]. Two-axis twisting (TAT) [9,19–23], which is performed simultaneously clockwise and counterclockwise twisting around two orthogonal axes, can generate spin squeezed states with a fixed optimal squeezing angle during the twisting evolution [9]. The corresponding phase estimation uncertainty is proportional to N^{-1} , which can exhibit the Heisenberg scaling [5]. However, the TAT interaction has

not yet been found directly in any known physical systems. To facilitate an effective TAT interaction, one can transform OAT into TAT by applying well-designed sequences of transverse coherent fields [12,24–29].

Apart from entanglement generation, state detection is also important in quantum metrology. The detection of highly entangled states generally requires single-particle resolved detection. To relax the stringent requirement of low-noise detection, interaction-based readout [16,30–54] has been proposed in recent years. It provides a powerful way for approaching the precision bound of the Heisenberg limit. It is of broad interest to explore time-reversal echoes based on the OAT [32] and TAT [33]. In particular for spin squeezed states, using the time-reversal echo dynamics [31–35] as interaction-based readout enables the Heisenberg-limited precision. However, it is necessary to reverse the quantum dynamics of an interacting many-body system, which is typically realized by flipping the sign of interaction. Despite the fact that the time-reversal echoes based on OAT [55] and twist-and-turn [56] have been demonstrated with cold atoms in an optical cavity, it is still experimentally challenging to flip the sign of interaction in other systems [33], such as BECs [13,14]. Therefore, a natural question arises: can one achieve an effective TAT echo scheme without flipping the sign of interaction?

In this paper, we propose an echo protocol based on synthetic TAT from interaction-fixed OAT in a pseudospin-1/2 ensemble. By applying modulation pulses around two different orthogonal directions, the effective TAT and its echo, i.e., an effective two-axis antitwisting (TAAT), can be realized respectively without flipping the sign of the OAT interaction. Our results show that, using the synthetic two-axis-twisting

*Contact author: hjihao@mail2.sysu.edu.cn, ejjihao@gmail.com†Contact author: chleecn@szu.edu.cn, chleecn@gmail.com

echo (STATE) protocol for phase estimation, one can not only obtain larger metrological gain than that by using OAT echo, but also require a shorter evolution time, even in the presence of detection noises. The effects of pulse imperfections are also considered, and our protocol is somewhat robust against pulse imperfections. Our protocol can realize the effective TAT echo scheme without flipping the sign of interaction, thus proving a practical way for realizing robust high-precision phase estimation.

II. REALIZATION OF THE SYNTHETIC TWO-AXIS-TWISTING ECHO SCHEME

We consider a collective spin system with N spins occupying two different energy levels $|\uparrow\rangle$ and $|\downarrow\rangle$. It is convenient to describe the system by collective spin operators $\hat{J}_\mu = \sum_{k=1}^N \hat{\sigma}_k^{(\mu)}/2$, where $\hat{\sigma}_k^{(\mu)}$ are Pauli operators for the k th particle with $\mu = x, y, z$. The TAT Hamiltonian (we set $\hbar = 1$ hereafter) can be written as $\hat{H}_{\text{TAT}} = \chi'(\hat{J}_x^2 - \hat{J}_y^2)$, where χ' indicates the TAT nonlinear interaction strength. Before introducing how to realize our STATE scheme, we first briefly introduce the echo scheme based on the original TAT [33].

The implementation process of a general echo scheme can be expressed as $|\psi_f\rangle = \hat{R}_m \hat{U}_2 \hat{R}_n(\phi) \hat{U}_1 |\psi_i\rangle$. At first, the initial state is generally prepared in a spin coherent state (SCS) polarized along the z axis, i.e., $|\psi_i\rangle = |\uparrow\rangle^{\otimes N}$. Second, the entangled spin state is dynamically generated by $\hat{U}_1 = e^{-i\hat{H}_{\text{TAT}}T}$ with T the evolution time. Third, the phase encoding along $\hat{J}_\alpha = \frac{\sqrt{2}}{2}(\hat{J}_x - \hat{J}_y)$ direction $\hat{R}_n(\phi) = e^{-i\phi\hat{J}_\alpha}$ is performed. Then, the antitwisting $\hat{U}_2 = \hat{U}_1^\dagger = e^{i\hat{H}_{\text{TAT}}T}$ is implemented to recover back to a closely resembled SCS, resulting in a large displacement $\langle \hat{J}_\beta \rangle$ with $\hat{J}_\beta = \frac{\sqrt{2}}{2}(\hat{J}_x + \hat{J}_y)$. Finally, one can rotate the state with $\hat{R}_m = e^{-i\hat{J}_y\pi/2} e^{i\hat{J}_z\pi/4}$ and applying half-population difference measurement $\langle \hat{J}_z \rangle$ to extract the information of ϕ .

For realizing our STATE scheme, we consider adding the linear coupling $\Omega_1(t)\hat{J}_y$ (along y axis) into the OAT Hamiltonian $\hat{H}_{\text{OAT}} = \chi\hat{J}_z^2$ for twisting [25] and adding the linear coupling $\Omega_2(t)\hat{J}_x$ (along x axis) into the OAT Hamiltonian for antitwisting, i.e.,

$$\hat{H}_{\text{twist}}(t) = \chi\hat{J}_z^2 + \Omega_1(t)\hat{J}_y \quad (1)$$

and

$$\hat{H}_{\text{antitwist}}(t) = \chi\hat{J}_z^2 + \Omega_2(t)\hat{J}_x, \quad (2)$$

where the fixed χ stands for the OAT nonlinear interaction strength, while the time-varying $\Omega_1(t)$ and $\Omega_2(t)$ are the linear coupling amplitudes during twisting and antitwisting, respectively. Hereafter, we assume the couplings are achieved by short pulses. When the coupling pulses are switched on, we set $\Omega_1(t) = \Omega_2(t) = \Omega$, satisfying $|\Omega| \gg \chi N$. In this case, linear coupling dominates and nonlinear interaction can be ignored. While coupling pulses are turned off, $\Omega_1(t) = \Omega_2(t) = 0$, it is reduced to the OAT dynamics.

Then, we show how to achieve the TAT evolution $e^{-i\chi(\hat{J}_x^2 - \hat{J}_y^2)t}$ and the TAAT evolution $e^{-i\chi(\hat{J}_y^2 - \hat{J}_x^2)t}$ by applying pulses based on interaction-fixed OAT. Assume the total collective spin $\hat{J}^2 = \hat{J}_x^2 + \hat{J}_y^2 + \hat{J}_z^2$ is conserved during the time evolution. Thus, up to a constant phase factor, the

TAT evolution $e^{-i\chi(\hat{J}_x^2 - \hat{J}_y^2)t}$ can be written as $e^{-i\chi(\hat{J}^2 + \hat{J}_x^2 - \hat{J}_y^2)t} = e^{-i\chi(2\hat{J}_z^2 + \hat{J}_x^2)t}$, and the TAAT evolution $e^{-i\chi(\hat{J}_y^2 - \hat{J}_x^2)t}$ also can be written as $e^{-i\chi(\hat{J}^2 + \hat{J}_y^2 - \hat{J}_x^2)t} = e^{-i\chi(2\hat{J}_z^2 + \hat{J}_y^2)t}$. When $\eta = \chi\Delta t$ is small enough, the TAT and TAAT can be approximately decomposed into OAT and linear rotations around different axes. Using the second-order Trotter-Suzuki expansion [25], we have

$$e^{-i\eta(\hat{J}_x^2 - \hat{J}_y^2)} \simeq e^{-i\frac{\eta}{2}\hat{J}_z^2} e^{-i2\eta\hat{J}_x^2} e^{-i\frac{\eta}{2}\hat{J}_z^2} + O[(-i\eta)^3], \quad (3)$$

$$e^{-i\eta(\hat{J}_y^2 - \hat{J}_x^2)} \simeq e^{-i\frac{\eta}{2}\hat{J}_z^2} e^{-i2\eta\hat{J}_y^2} e^{-i\frac{\eta}{2}\hat{J}_z^2} + O[(-i\eta)^3]. \quad (4)$$

For achieving the OAT around the x and y axis, the pulses should be applied to rotate $e^{-i\chi\hat{J}_z^2 t}$ to $e^{-i\chi\hat{J}_x^2 t}$ or to $e^{-i\chi\hat{J}_y^2 t}$ as follows:

$$\hat{R}_{-\pi/2}^y e^{-i\chi\hat{J}_z^2 t} \hat{R}_{+\pi/2}^y = e^{-i\chi\hat{J}_x^2 t}, \quad (5)$$

$$\hat{R}_{-\pi/2}^x e^{-i\chi\hat{J}_z^2 t} \hat{R}_{+\pi/2}^x = e^{-i\chi\hat{J}_y^2 t}, \quad (6)$$

where the $\pm\pi/2$ rotation operators are defined as $\hat{R}_{\pm\pi/2}^y = e^{\mp i\pi\hat{J}_y/2}$ and $\hat{R}_{\pm\pi/2}^x = e^{\mp i\pi\hat{J}_x/2}$, respectively. Combining Eqs. (3) and (5), we arrive at

$$e^{-i\eta(\hat{J}_x^2 - \hat{J}_y^2)} \approx e^{-i\frac{\eta}{2}\hat{J}_z^2} \hat{R}_{-\pi/2}^y e^{-i2\eta\hat{J}_x^2} \hat{R}_{+\pi/2}^y e^{-i\frac{\eta}{2}\hat{J}_z^2}, \quad (7)$$

and combining Eqs. (4) and (6), we arrive at

$$e^{-i\eta(\hat{J}_y^2 - \hat{J}_x^2)} \approx e^{-i\frac{\eta}{2}\hat{J}_z^2} \hat{R}_{-\pi/2}^x e^{-i2\eta\hat{J}_y^2} \hat{R}_{+\pi/2}^x e^{-i\frac{\eta}{2}\hat{J}_z^2}. \quad (8)$$

Equations (7) and (8) indicate that the TAT and TAAT evolution can be implemented approximately via the Hamiltonian in Eqs. (1) and (2) by using $\pi/2$ -pulse sequences along y and x direction, respectively.

Specifically, we show how to realize the synthetic two-axis twisting (STAT) and synthetic two-axis antitwisting (STAAT) in a small period. The whole period can be divided into three parts. The STAT, as shown in the top of Fig. 1(a), can be realized through implementing the first OAT evolution lasting $\delta t/2$, subsequently applying a $+\pi/2$ pulse (red pulse) along y followed by the second OAT evolution lasting $2\delta t$, and finally applying another $-\pi/2$ pulse (blue pulse) along y followed by the third OAT evolution lasting $\delta t/2$. Thus, the STAT evolution for such a single period $\Delta t = 3\delta t$ can be expressed as

$$\hat{U}_a = e^{-i\chi\frac{\delta t}{2}\hat{J}_z^2} \hat{R}_{-\pi/2}^y e^{-i\chi 2\delta t\hat{J}_z^2} \hat{R}_{+\pi/2}^y e^{-i\chi\frac{\delta t}{2}\hat{J}_z^2}. \quad (9)$$

The operation for realizing the STAAT evolution is similar with the STAT evolution, except that the first $+\pi/2$ pulse (orange pulse) and the second $-\pi/2$ pulse (green pulse) are along x , as shown in the bottom of Fig. 1(a). Thus the STAAT evolution for such a single period Δt can be written as

$$\hat{U}_b = e^{-i\chi\frac{\delta t}{2}\hat{J}_z^2} \hat{R}_{-\pi/2}^x e^{-i\chi 2\delta t\hat{J}_z^2} \hat{R}_{+\pi/2}^x e^{-i\chi\frac{\delta t}{2}\hat{J}_z^2}. \quad (10)$$

The above operations constitute the STAT or STAAT for a single period of Δt . Repeating these operations for N_c periods, one can obtain the evolution of STAT or STAAT for a total evolution time $T = N_c\Delta t$. Therefore, the evolution operators for twisting and antitwisting can be given by $\hat{U}_1(T) = (\hat{U}_a)^{N_c}$ and $\hat{U}_2(T) = (\hat{U}_b)^{N_c}$, respectively. For a given evolution time T , when the interval of a single period is short enough $\Delta t \rightarrow 0$, the evolution operators for TAT and TAAT can

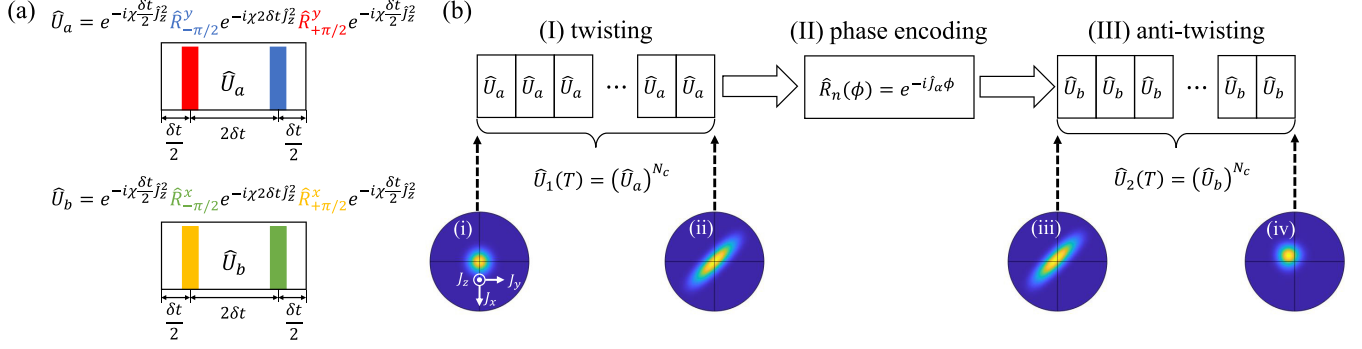


FIG. 1. (a) The implementation of the pulse sequence to realize STAT and STAAT in a short period, consisting of rotations $\hat{R}_{\pm\pi/2}^y$ (+, red pulse; -, blue pulse) and rotations $\hat{R}_{\pm\pi/2}^x$ (+, orange pulse; -, green pulse), respectively. (b) Schematic diagram of the STATE protocol. The upper panel shows the implementation process of the STATE protocol, which includes (I) the periodic pulse sequences to realize STAT, (II) phase encoding, and (III) the periodic pulse sequences to realize STAAT. The lower panel shows the evolved states in each stage, visualized by Husimi distribution on the generalized Bloch spheres. (i) In the beginning, the state is prepared in an unentangled state with all spins polarized along z , (ii) then the entangled state is obtained after the STAT which includes N_c periods of pulse sequence \hat{U}_a , (iii) subsequently the entangled state encodes the estimated phase around $\hat{J}_\alpha = \frac{\sqrt{2}}{2}(\hat{J}_x - \hat{J}_y)$ direction, and (iv) finally the state is recovered as nearly a SCS with large displacement along $\hat{J}_\beta = \frac{\sqrt{2}}{2}(\hat{J}_x + \hat{J}_y)$ direction after the STAAT which includes N_c periods of pulse sequence \hat{U}_b . The final state is rotated as $\hat{R}_m = e^{-i\hat{J}_y\pi/2} e^{i\hat{J}_z\pi/4}$ in order to transfer the large displacement to the z direction before the half-population difference measurement.

be represented exactly as $\hat{U}_1 = e^{-i(\hat{J}_x^2 - \hat{J}_y^2)\chi T/3}$, and $\hat{U}_2 = e^{-i(\hat{J}_y^2 - \hat{J}_x^2)\chi T/3}$, respectively. Therefore, the effective Hamiltonian for STAT is

$$\hat{H}_1^{\text{eff}} = \frac{\chi}{3} (\hat{J}_x^2 - \hat{J}_y^2), \quad (11)$$

and the one for STAAT is

$$\hat{H}_2^{\text{eff}} = \frac{\chi}{3} (\hat{J}_y^2 - \hat{J}_x^2). \quad (12)$$

It is important to emphasize that the OAT interaction strength χ is fixed throughout the time evolution.

Therefore, as shown in Fig. 1(b), our STATE scheme can be implemented as follows:

$$|\psi_f\rangle = \hat{R}_m (\hat{U}_b)^{N_c} \hat{R}_n(\phi) (\hat{U}_a)^{N_c} |\psi_i\rangle. \quad (13)$$

At first, the initial state $|\psi_i\rangle$ is prepared in a SCS polarized along z . Then, the entangled spin state is achieved via implementing synthetic TAT $(\hat{U}_a)^{N_c}$. Subsequently, the phase encoding $\hat{R}_n(\phi) = e^{-i\phi\hat{J}_\alpha}$ is around the $\hat{J}_\alpha = \frac{\sqrt{2}}{2}(\hat{J}_x - \hat{J}_y)$ direction. Finally, the synthetic TAAT $(\hat{U}_b)^{N_c}$ is implemented to recover back to a near SCS, resulting in a large displacement $\langle\hat{J}_\beta\rangle$ with $\hat{J}_\beta = \frac{\sqrt{2}}{2}(\hat{J}_x + \hat{J}_y)$ (see Fig. 1). To perform the half-population difference measurement, we rotate the state with $\hat{R}_m = e^{-i\hat{J}_y\pi/2} e^{i\hat{J}_z\pi/4}$. Thus, one can achieve an effective TAT echo protocol from interaction-fixed OAT by only applying a sequence of pulses.

III. METROLOGICAL GAIN

In this section, we first introduce the metrological gain for estimating the phase sensitivity and compare the four echo schemes, including the OAT echo, synthetic OAT (SOAT) echo, TAT echo, and STATE schemes. In Sec. III A, we study the effects of pulse number on the metrological gain, and consequently find out the required number of pulses for realizing the metrological gain over OAT and close to the

TAT echo scheme. The effect of phase accumulation on the metrological gain is investigated in Sec. III B. The small signal phase is amplified via an echo leading to the improved signal response to phase. Consequently, the metrological gain obtained with echo is larger than that without echo. In Sec. III C, the influences of pulse imperfections on metrological gain are investigated which include the pulse strength, the uncertainty of pulse area, the uncertainty of pulse action time, and the uncertainty of pulse switch-on and -off time. In Sec. III D, the effects of detection noise on metrological gain are studied, in which the pulse imperfections are considered. Finally, the scaling of metrological gain with particle number is shown in Sec. III E, where the pulse imperfections and the detection noise are considered simultaneously.

After implementing our STATE scheme, the last and most important step is to evaluate the phase sensitivity. The phase sensitivity can be estimated via the error propagation formula after performing the half-population difference measurement

$$\Delta\phi = \frac{\Delta\hat{J}_z}{|\partial_\phi\langle\hat{J}_z\rangle|}, \quad (14)$$

where $\langle\hat{J}_z\rangle = \langle\psi_f|\hat{J}_z|\psi_f\rangle$ and $\Delta\hat{J}_z = \sqrt{\langle\hat{J}_z^2\rangle - \langle\hat{J}_z\rangle^2}$ represent the mean and standard deviation of \hat{J}_z , and $\partial_\phi\langle\hat{J}_z\rangle = \partial\langle\hat{J}_z\rangle/\partial\phi$ denotes the signal response to phase. To compare with the SQL phase sensitivity, the metrological gain is formally defined as

$$G = 20 \log_{10} \left[\frac{(\Delta\phi)_{\text{SQL}}}{\Delta\phi} \right] = 20 \log_{10} \left(\frac{|\partial_\phi\langle\hat{J}_z\rangle|}{\sqrt{N}\Delta\hat{J}_z} \right), \quad (15)$$

where $(\Delta\phi)_{\text{SQL}} = 1/\sqrt{N}$ denotes the phase sensitivity of SQL.

Below, we compare the four echo schemes, including the OAT echo, SOAT echo, TAT echo, and STATE schemes [32,33]. We first introduce the implementation process of the OAT echo, SOAT echo, and TAT echo schemes. The

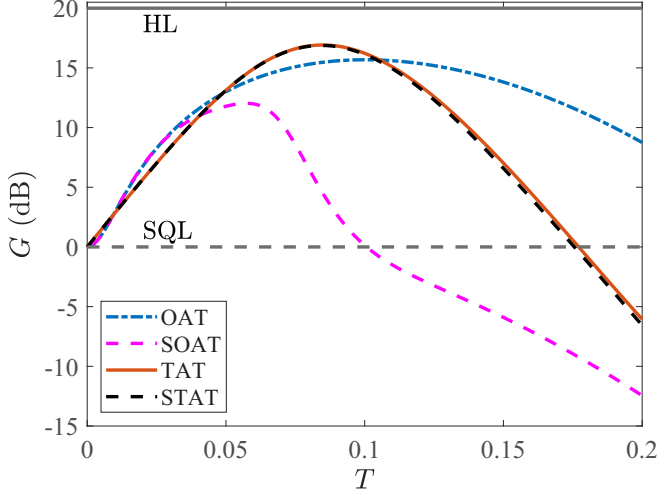


FIG. 2. Dependence of metrological gain on evolution time T with OAT, SOAT, TAT, and STAT echo schemes. For the STATE scheme, $N_c = 30$. The particle number is chosen as $N = 100$ in our simulations. The gray solid (dashed) line represents the HL (SQL).

implementation process of the OAT echo scheme is $|\psi_f\rangle = \hat{R}_m \hat{U}_2 \hat{R}_n(\phi) \hat{U}_1 |\psi_i\rangle$. The initial state $|\psi_i\rangle$ is chosen as an SCS polarized along x . The phase encoding $\hat{R}_n(\phi) = e^{-i\hat{J}_y \phi}$ is along the y direction. The echo dynamics is implemented as $\hat{U}_2 = \hat{U}_1^\dagger$ with $\hat{U}_1 = e^{-i\hat{H}_{\text{OAT}} T}$ and $\hat{H}_{\text{OAT}} = \chi \hat{J}_z^2$. Finally, we implement the rotation $\hat{R}_m = e^{i\hat{J}_x \varphi}$ to perform the half-population difference measurement, in which φ is chosen to provide the largest metrological gain among all possible values. The time-reversal echo of OAT is realized via flipping the sign of many-body interaction. To compare with the STAT echo scheme in the same system where no sign change is possible, we also consider the SOAT echo scheme, whose implementation process is $|\psi_f\rangle = \hat{R}_m \hat{U}_1 \hat{R}_n(\phi) \hat{R}_x(\theta) \hat{U}_1 |\psi_i\rangle$. Different from the OAT echo scheme, a rotation along the x axis is applied via $\hat{R}_x(\theta) = e^{-i\hat{J}_x \theta}$ with $\theta = \pi - 2\gamma_{\text{opt}}$ before the phase encoding and the sign of the Hamiltonian is left unchanged. Here, $\gamma_{\text{opt}} = \frac{1}{2} \arctan(B/A)$ is the optimal angle of squeezing for OAT, in which $A = 1 - \cos^{N-2}(2\chi t)$ and $B = 4 \cos^{N-2}(\chi t) \sin(\chi t)$ [9]. Further, to verify that the STAT echo scheme is equivalent to the TAT echo scheme, the TAT echo scheme is also considered. Different from the STATE schemes, the dynamical evolution for the TAT echo scheme is $\hat{U}_1 = e^{-i\hat{H}_{\text{TAT}} T}$ with $\hat{H}_{\text{TAT}} = \chi(\hat{J}_x^2 - \hat{J}_y^2)/3$ and time-reversal echo $\hat{U}_2 = \hat{U}_1^\dagger$ is achieved by flipping the sign of the Hamiltonian.

We study the dependence of metrological gain on the evolution time T for the STATE scheme, and compare with the OAT echo, STAT echo, and TAT echo schemes, as shown in Fig. 2. In our simulation ($N = 100$, $\chi = 1$, $N_c = 30$), for the STATE scheme (black dashed line), the maximal metrological gain $G_{\text{max}}^{\text{STAT}} \approx 16.88$ is achieved at the optimal evolution time $T_{\text{opt}}^{\text{STAT}} = 0.0795$, near the time $3 \ln(2N)/(2N\chi)$ [19], and for the OAT echo scheme (blue dash-dotted line), the maximal metrological gain $G_{\text{max}}^{\text{OAT}} \approx 15.63$ is achieved at the optimal evolution time $T_{\text{opt}}^{\text{OAT}} = 0.1$, corresponding to the time $1/(\chi\sqrt{N})$ [32]. The result of the STAT echo is consistent with

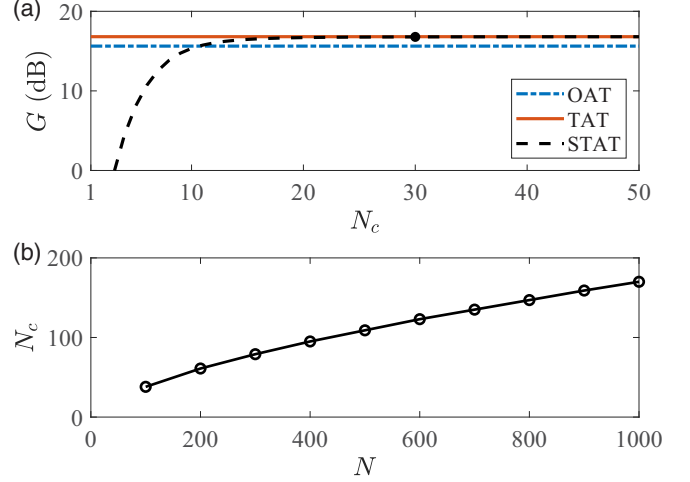


FIG. 3. (a) Dependence of metrological gain on the number of periods N_c for the STATE scheme implemented with optimal evolution time. The blue dash-dotted and orange solid lines represent metrological gain obtained via the OAT and TAT echo schemes implemented at near optimal evolution time. The particle number is chosen as $N = 100$ in our simulations. (b) The minimum required number of periods N_c satisfying $G_{\text{TAT}} - G_{\text{STAT}} < 0.01$ for different particle number.

the one of the TAT echo when $N_c = 30$, and the result of the SOAT echo is consistent with the one of the OAT echo within short evolution time. Compared to the OAT echo scheme, the STAT echo scheme has a larger maximum achievable metrological gain and a faster evolution time. Furthermore, when compared to the SOAT echo scheme in the same system, which does not allow for sign changes, the STATE scheme also shows a larger maximum available metrological gain, which is more effective and feasible for experiments.

A. Effects of pulse number

Since the STATE scheme is implemented by applying a sequence of periodic pulses, the phase measurement precision is bound to be affected by the pulse number. Here, we study the effects of the pulse number on the metrological gain obtained via our STATE scheme. In theory, Eq. (3) illustrates that the validity of STAT depends on $\eta = \chi \Delta t$. Considering the total evolution time T is fixed and divided into N_c periods, the single period is $\Delta t = T/N_c$. To ensure $\Delta t \rightarrow 0$, the total number of periods $N_c \rightarrow \infty$, i.e., the total number of pulses $N_p = 4N_c \rightarrow \infty$. Therefore, a greater number of pulses is better to achieve the effective TAT.

However, the available number of pulses may be limited in practical experiments. Below, we investigate the dependence of metrological gain on the number of total periods N_c for the STATE scheme implemented with optimal evolution time $T = 3 \ln(2N)/(2N\chi)$ by numerical simulation, and the results are shown in Fig. 3(a). As the number of pulses N_p increases, the metrological gain also increases. For both the OAT echo (blue dash-dotted line) and TAT (orange solid line) echo schemes, the corresponding optimal metrological gains are chosen for comparison. For $N = 100$, when the number of periods increases to $N_c = 11$, i.e., the number of pulses

increases to $N_p = 44$, the metrological gain of the STATE scheme exceeds that of the OAT echo scheme. Further, when the number of periods increases to $N_c = 20$, i.e., $N_p = 80$, the metrological gain of the STATE scheme is very close to that of the TAT echo scheme. According to our simulation, for the case of $N = 100$ particles, applying $N_p = 120$ pulses is sufficient.

For different particle number N , we investigate the minimum required number of periods N_c satisfying $G_{\text{TAT}} - G_{\text{STAT}} < 0.01$, where G_{TAT} and G_{STAT} stand for the metrological gain obtained via the TAT echo and STATE scheme at the optimal evolution time $T = 3 \ln(2N)/(2N\chi)$, respectively. As the number of particles grows, the corresponding evolution time decreases, and the number of required N_c increases, as shown in Fig. 3(b).

B. Effects of phase accumulation

Here, we investigate the effects of phase accumulation. In practice, the value of the estimated phase influences the metrological gain of the echo protocols. The minimal achievable uncertainty of the estimated phase is theoretically determined by the quantum Cramér-Rao bound (QCRB) [6], expressed as $(\Delta\phi)_{\text{QCRB}} = 1/\sqrt{F_Q}$, where the quantum Fisher information can be calculated as $F_Q = 4(\Delta\hat{J}_\alpha)^2$ [57,58]. The corresponding metrological gain for the QCRB is denoted as $G_Q = 20 \log_{10}[(\Delta\phi)_{\text{SQL}}/(\Delta\phi)_{\text{QCRB}}]$. In practice, it proves immensely beneficial to extract the achievable uncertainty close to the QCRB through population measurement.

We show the normalized signal $P = \langle \hat{J}_z \rangle / N + 1/2$ for OAT, TAT, and STAT echoes in Fig. 4(a). The contrast is defined as $C = (P_{\text{max}} - P_{\text{min}})/(P_{\text{max}} + P_{\text{min}})$, with OAT and STAT being $C = 0.688$ and 0.639 , respectively. Although the STATE scheme suffers a slight contrast loss compared with the OAT echo scheme, a higher metrological gain can be achieved. Figure 4(b) demonstrates the metrological gain obtained via our STATE scheme at the optimal evolution time for encoding different estimated phases. Notably, the result indicates that significant metrological gain can be achieved via the STATE scheme (purple dash-dotted line) for a tiny estimated phase through population measurement, closely approaching the QCRB when the accumulated phase $\phi \approx 0$. In contrast, the achievable uncertainty obtained without the echo process (pink dashed line) significantly deviates from the QCRB.

To elucidate why the echo scheme nearly saturates the QCRB, we examine the signal $\langle \hat{J}_z \rangle$ [Fig. 4(c)], signal response to phase $|\partial_\phi \langle \hat{J}_z \rangle|$ [Fig. 4(d)], and quantum projection noise $\Delta\hat{J}_z$ [Fig. 4(e)]. The phase sensitivity is determined by the noise $\Delta\hat{J}_z$ and the signal response to phase $|\partial_\phi \langle \hat{J}_z \rangle|$. Although the noise $\Delta\hat{J}_z$ based on the echo process surpasses the one without the echo process, the signal response to phase $|\partial_\phi \langle \hat{J}_z \rangle|$ is in the meantime significantly amplified. This substantial amplification of the signal response to phase originates from phase signal amplification of $\langle \hat{J}_z \rangle$. Consequently, the phase sensitivity nearly saturating the QCRB is facilitated through phase amplification.

C. Effects of pulse imperfections

Up to this point, we have primarily dealt with ideal pulses that simply rotate the quantum state by a phase shift of $\pi/2$

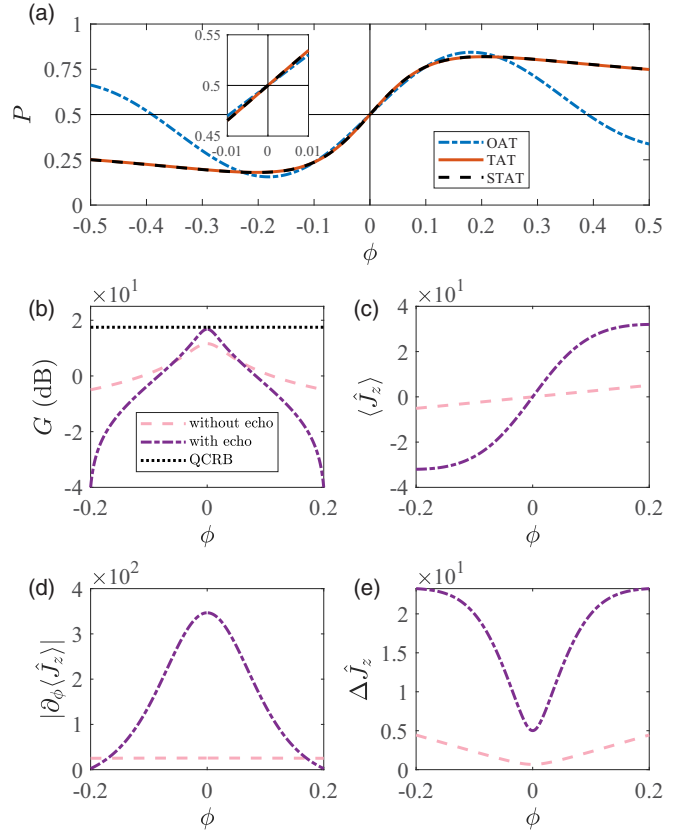


FIG. 4. (a) The normalized signal $P = \langle \hat{J}_z \rangle / N + 1/2$ for OAT, TAT, and STAT echoes implemented at optimal evolution time. The inset shows the results in the range of $\phi \in [-0.01, 0.01]$. Dependence of (b) metrological gain, (c) signal $\langle \hat{J}_z \rangle$, (d) signal response to phase $|\partial_\phi \langle \hat{J}_z \rangle|$, and (e) standard deviation of the signal $\Delta\hat{J}_z$ on the rotation angle ϕ for the STATE scheme implemented at optimal evolution time. Purple dash-dotted and pink dashed lines are the cases with and without echo, respectively. Black dotted line represents the metrological gain corresponding to the QCRB. Here, the particle number $N = 100$ and the number of periods $N_c = 30$ in our simulations.

about the x or y axis. However, in practical experiments, the applied pulses are not perfect. In the following, four types of the pulse imperfections within our STATE scheme are discussed.

First, alongside the pulse action, the interaction term $\chi\hat{J}_z^2$ may have an influence. For the required $\pi/2$ pulses, a stronger pulse intensity implies a shorter pulse duration and consequently reduces the impact of the interaction term. The dependence of metrological gain on the pulse Rabi frequency is shown in Fig. 5(a). When the Rabi frequency is larger than a threshold, the metrological gain saturates.

Additionally, the area of the pulse may not be exactly $\pi/2$ in experiments. Hence, we consider that the area of the applied pulse has a Gaussian random distribution $\mathcal{N}(\pi/2, \sigma_p)$, where σ_p is the standard deviation. To account for the variability inherent in Gaussian distribution sampling, we conduct 100 numerical simulations. The impact of pulse area uncertainty on metrological gain is shown in Fig. 5(b). The mean value is denoted by a point with error bars indicating the standard

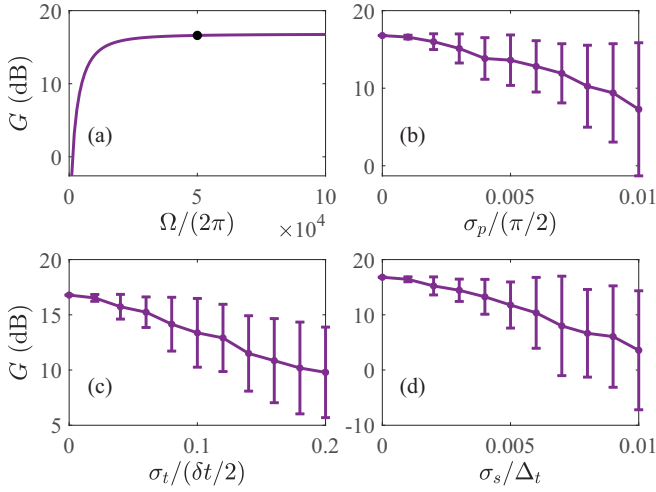


FIG. 5. Effects of pulse imperfections on the metrological gain including (a) pulse Rabi frequency, (b) uncertainty of pulse area, (c) uncertainty of pulse action time, and (d) uncertainty of pulse switch-on and -off time.

deviation. As the uncertainty of pulse area increases, metrological gain decreases.

Furthermore, the timing of pulse action in our scheme is also crucial. We assume the pulse action time follows a Gaussian random distribution $\mathcal{N}(t_a, \sigma_t)$, where t_a and σ_t represent the expected value and standard deviation of each perfect pulse action time, respectively. Figure 5(c) displays the dependence of metrological gain on the uncertainty of pulse action time. Here, $\delta t/2$ represents the first pulse action time in each period. As the uncertainty of pulse action time increases, metrological gain also decreases.

So far, we have separately examined the effects of pulse Rabi frequency, pulse area uncertainty, and pulse action time uncertainty on metrological gain. However, in practical experiments, these effects may occur simultaneously. After selecting a sufficiently strong pulse, the only remaining control factor is the timing of pulse activation and deactivation. Therefore, uncertainty in these timings leads to indeterminate phase application by the pulse. Here, we assume that the pulse switch-on and switch-off times follow Gaussian random distributions $\mathcal{N}(t_{\text{on}}, \sigma_s)$ and $\mathcal{N}(t_{\text{off}}, \sigma_s)$, respectively. Figure 5(d) illustrates the dependence of metrological gain on the uncertainty of pulse activation and deactivation times. Here, $\Delta_t = \pi/(2\Omega)$ denotes the time interval for pulse activation and deactivation, where Ω is chosen as $2\pi \times 50$ kHz, as shown by the black dot marked in Fig. 5(a). Although the pulse imperfection reduces the metrological gain, the SQL can still be broken within a certain range. Through our calculations, the metrological gain can remain high if one can control σ_s below $0.005\Delta_t$.

D. Effects of detection noise

In practical experiments, other experimental imperfections also significantly affect the precision of the final phase estimation [59–61]. In particular, detection noise is a critical factor influenced by the detector's performance, leading to inaccurate particle counting [32,37,40,62]. In this subsection,

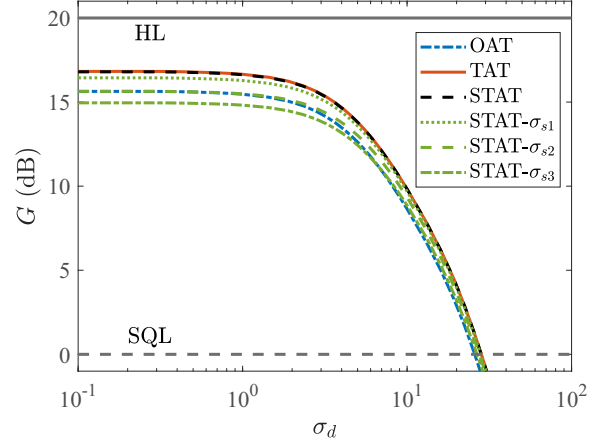


FIG. 6. Metrological gain G vs the magnitude of detection noise σ_d . All echo schemes are implemented with corresponding optimal evolution time. For the STATE scheme, the uncertainty of pulse switch-on and -off time is also considered with $\sigma_{s1} = 0.001\Delta_t$ (green dot line), $\sigma_{s2} = 0.002\Delta_t$ (green dashed line), and $\sigma_{s3} = 0.003\Delta_t$ (green dash-dotted line). Here, we choose the particle number $N = 100$ and the number of periods $N_c = 30$ in our simulations.

we aim to investigate the robustness of our STATE scheme against detection noise and compare it with the OAT echo and TAT echo schemes.

Half-population difference is commonly selected as the observable for the final state due to its practical implementation. Ideally, the measurement result can be expressed as $\langle \hat{J}_z \rangle = \sum_{m=-N/2}^{N/2} P_m(\phi) m$, where $P_m(\phi)$ represents the measured probability of the final state projecting onto the basis $|J, m\rangle$. However, for an inefficient detector with Gaussian detection noise [40], the half-population difference measurement may become

$$\langle \hat{J}_z \rangle_{\sigma_d} = \sum_{m=-N/2}^{N/2} P_m(\phi | \sigma_d) m, \quad (16)$$

where $P_m(\phi | \sigma_d)$ is the probability distribution considering the detection noise, defined as

$$P_m(\phi | \sigma_d) = \sum_{n=-N/2}^{N/2} A_n e^{-(m-n)^2/2\sigma_d^2} P_n(\phi), \quad (17)$$

with $A_n = 1/\sum_{m=-N/2}^{N/2} e^{-(m-n)^2/2\sigma_d^2}$ being the normalization factor.

We depict the metrological gain versus the magnitude of detection noise in Fig. 6 for STATE schemes, considering both perfect and imperfect pulses. The imperfect pulses account for the uncertainty of pulse switch-on and -off times as previously. Results for STATE schemes with different pulse imperfections ($\sigma_{s1} = 0.001\Delta_t$, $\sigma_{s2} = 0.002\Delta_t$, and $\sigma_{s3} = 0.003\Delta_t$) are averaged over 100 simulations and represented by green dot line, green dashed line, and green dash-dotted line, respectively.

In addition, the results for OAT echo and TAT echo schemes are presented for comparison, with all echo schemes implemented at corresponding optimal evolution time and a chosen number of periods $N_c = 30$ for the STATE scheme.

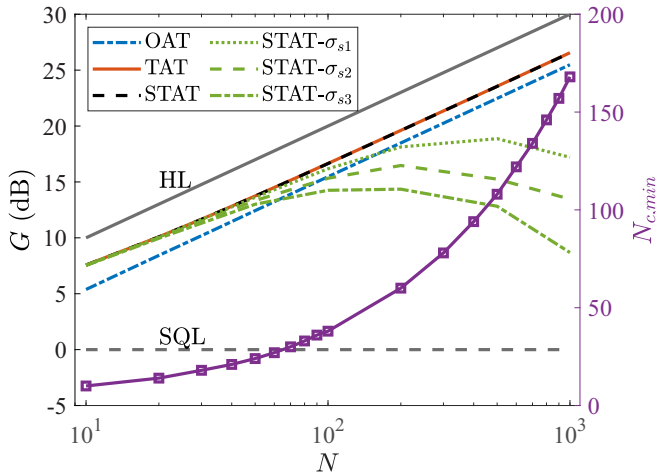


FIG. 7. The scaling of metrological gain vs the particle number N . All echo schemes are implemented with the corresponding optimal time under detection noise $\sigma_d = \sqrt{N}/10$. The minimum required number of periods $N_{c,\min}$ (purple square marker) which are used for all STATE schemes satisfying $G_{\text{TAT}} - G_{\text{STAT}} < 0.01$ is shown on the right.

Remarkably, for all echo schemes, the metrological gain remains nearly unchanged below $\sigma_d = \sqrt{N}/10$, and even surpasses the SQL under large detection noise, indicating the effectiveness of echo protocols in enhancing robustness to detection noise. For perfect pulses, the metrological gain obtained via the STATE scheme outperforms that via the OAT echo scheme with the same detection noise. This demonstrates that the STATE scheme is not only robust against detection noise but also superior to the OAT echo scheme under the same detection noise. Conversely, for imperfect pulses, the performance of the STATE scheme with $\sigma_{s1} = 0.001\Delta_t$ surpasses that of the OAT echo scheme. The STATE scheme with $\sigma_{s2} = 0.002\Delta_t$ performs similarly to the OAT echo scheme under small detection noise but outperforms it under large detection noise. However, the STATE scheme with $\sigma_{s3} = 0.003\Delta_t$ performs worse than the OAT echo scheme under small detection noise, but outperforms it under large detection noise.

E. Scaling with respect to particle number

Finally, we examine the scaling of metrological gain versus particle number N with detection noise $\sigma_d = \sqrt{N}/10$ for the STATE scheme and compare it with the OAT echo and TAT echo schemes, as illustrated in Fig. 7. The results for STATE schemes with different pulse imperfections ($\sigma_{s1} = 0.001\Delta_t$, $\sigma_{s2} = 0.002\Delta_t$, and $\sigma_{s3} = 0.003\Delta_t$) are averaged over 100

simulations and depicted as green dotted, green dashed, and green dash-dotted lines, respectively. The pulse strengths for various particle numbers (10,20,50,100,200,500,1000) are represented by $\Omega = 2\pi \times (2, 5, 20, 100, 300, 5000, 10000)$ kHz. For implementing the STATE scheme with perfect pulses, we determine the minimum number of periods $N_{c,\min}$ satisfying $G_{\text{TAT}} - G_{\text{STAT}} < 0.01$. This $N_{c,\min}$ is used for the STATE scheme with both perfect and imperfect pulses, as shown in Fig. 7 with the purple line. All echo schemes are implemented with their corresponding optimal time.

The numerical results reveal that the STATE scheme utilizing perfect pulses adheres to Heisenberg scaling under detection noise $\sigma_d = \sqrt{N}/10$ and outperforms the OAT echo scheme. When considering the STATE scheme using imperfect pulses, the numerical findings indicate that schemes with different fluctuations at the moment when the pulse is turned on and off approximately adhere to Heisenberg scaling under small particle numbers. However, under large particle numbers, their metrological gains gradually deviate from Heisenberg scaling.

IV. CONCLUSION

In conclusion, we have proposed the synthetic two-axis-twisting echo protocol from interaction-fixed one-axis twisting for implementing entanglement-enhanced quantum metrology. Our protocol does not need to flip the sign of interaction for achieving time-reversal dynamics. We demonstrate that this protocol is not only robust against detection noise, but also outperforms the one-axis-twisting echo scheme with higher metrological gain and shorter evolution time. Further, this scheme can nearly saturate the ultimate precision bound and may approach the Heisenberg scaling even in the case with detection noise. In addition, we have carefully analyzed the effects of pulse imperfections which may occur in experiments. Our scheme may also be realized with continuous pulse driving [26], which can avoid the effects of pulse imperfections. Our protocol realizes the effective two-axis-twisting echo scheme without flipping the sign of interaction, thus proving a promising method for realizing higher precision and detection-noise-robust quantum metrology in various quantum many-body systems.

ACKNOWLEDGMENTS

The authors thank Yi Shen for critical reading and helpful suggestions. This work is supported by the National Key Research and Development Program of China (Grant No. 2022YFA1404104) and the National Natural Science Foundation of China (Grant No. 12025509).

- [1] V. Giovannetti, S. Lloyd, and L. Maccone, Quantum-enhanced measurements: Beating the standard quantum limit, *Science* **306**, 1330 (2004).
- [2] V. Giovannetti, S. Lloyd, and L. Maccone, Quantum metrology, *Phys. Rev. Lett.* **96**, 010401 (2006).
- [3] C. Lee, Adiabatic Mach-Zehnder interferometry on a quantized Bose-Josephson junction, *Phys. Rev. Lett.* **97**, 150402 (2006).

- [4] V. Giovannetti, S. Lloyd, and L. Maccone, Advances in quantum metrology, *Nat. Photon.* **5**, 222 (2011).
- [5] J. Ma, X. Wang, C. Sun, and F. Nori, Quantum spin squeezing, *Phys. Rep.* **509**, 89 (2011).
- [6] L. Pezzè, A. Smerzi, M. K. Oberthaler, R. Schmied, and P. Treutlein, Quantum metrology with nonclassical states of atomic ensembles, *Rev. Mod. Phys.* **90**, 035005 (2018).

- [7] C. L. Degen, F. Reinhard, and P. Cappellaro, Quantum sensing, *Rev. Mod. Phys.* **89**, 035002 (2017).
- [8] J. Huang, M. Zhuang, and C. Lee, Entanglement-enhanced quantum metrology: From standard quantum limit to Heisenberg limit, *Appl. Phys. Rev.* **11**, 031302 (2024).
- [9] M. Kitagawa and M. Ueda, Squeezed spin states, *Phys. Rev. A* **47**, 5138 (1993).
- [10] L.-G. Huang, F. Chen, X. Li, Y. Li, R. Lü, and Y.-C. Liu, Dynamic synthesis of Heisenberg-limited spin squeezing, *npj Quantum Inf.* **7**, 168 (2021).
- [11] L.-G. Huang, X. Zhang, Y. Wang, Z. Hua, Y. Tang, and Y.-C. Liu, Heisenberg-limited spin squeezing in coupled spin systems, *Phys. Rev. A* **107**, 042613 (2023).
- [12] Y. Wang, X. Zhang, and Y.-C. Liu, Spin squeezing through collective spin-spin interactions, [arXiv:2311.15667](https://arxiv.org/abs/2311.15667).
- [13] C. Gross, T. Zibold, E. Nicklas, J. Esteve, and M. K. Oberthaler, Nonlinear atom interferometer surpasses classical precision limit, *Nature (London)* **464**, 1165 (2010).
- [14] M. F. Riedel, P. Böhi, Y. Li, T. W. Hänsch, A. Sinatra, and P. Treutlein, Atom-chip-based generation of entanglement for quantum metrology, *Nature (London)* **464**, 1170 (2010).
- [15] H. Strobel, W. Muessel, D. Linnemann, T. Zibold, D. B. Hume, L. Pezzè, A. Smerzi, and M. K. Oberthaler, Fisher information and entanglement of non-Gaussian spin states, *Science* **345**, 424 (2014).
- [16] K. A. Gilmore, M. Affolter, R. J. Lewis-Swan, D. Barberena, E. Jordan, A. M. Rey, and J. J. Bollinger, Quantum-enhanced sensing of displacements and electric fields with two-dimensional trapped-ion crystals, *Science* **373**, 673 (2021).
- [17] I. D. Leroux, M. H. Schleier-Smith, and V. Vuletić, Implementation of cavity squeezing of a collective atomic spin, *Phys. Rev. Lett.* **104**, 073602 (2010).
- [18] G. P. Greve, C. Luo, B. Wu, and J. K. Thompson, Entanglement-enhanced matter-wave interferometry in a high-finesse cavity, *Nature (London)* **610**, 472 (2022).
- [19] D. Kajtch and E. Witkowska, Quantum dynamics generated by the two-axis counter-twisting Hamiltonian, *Phys. Rev. A* **92**, 013623 (2015).
- [20] C. Luo, H. Zhang, A. Chu, C. Maruko, A. M. Rey, and J. K. Thompson, Hamiltonian engineering of collective XYZ spin models in an optical cavity: From one-axis twisting to two-axis counter twisting models, [arXiv:2402.19429](https://arxiv.org/abs/2402.19429).
- [21] J. Borregaard, E. J. Davis, G. S. Bentsen, M. H. Schleier-Smith, and A. S. Sørensen, One- and two-axis squeezing of atomic ensembles in optical cavities, *New J. Phys.* **19**, 093021 (2017).
- [22] T. Hernández Yanes, M. Płodzień, M. Mackoiti Sinkevičienė, G. Žlabys, G. Juzeliūnas, and E. Witkowska, One- and two-axis squeezing via laser coupling in an atomic Fermi-Hubbard model, *Phys. Rev. Lett.* **129**, 090403 (2022).
- [23] L. Yu, C. Li, J. Fan, G. Chen, T.-C. Zhang, and S. Jia, Tunable two-axis spin model and spin squeezing in two cavities, *Chin. Phys. B* **25**, 050301 (2016).
- [24] Y. C. Liu, Z. F. Xu, G. R. Jin, and L. You, Spin squeezing: Transforming one-axis twisting into two-axis twisting, *Phys. Rev. Lett.* **107**, 013601 (2011).
- [25] J.-Y. Zhang, X.-F. Zhou, G.-C. Guo, and Z.-W. Zhou, Dynamical spin squeezing via a higher-order Trotter-Suzuki approximation, *Phys. Rev. A* **90**, 013604 (2014).
- [26] W. Huang, Y.-L. Zhang, C.-L. Zou, X.-B. Zou, and G.-C. Guo, Two-axis spin squeezing of two-component Bose-Einstein condensates via continuous driving, *Phys. Rev. A* **91**, 043642 (2015).
- [27] L.-N. Wu, M. K. Tey, and L. You, Persistent atomic spin squeezing at the Heisenberg limit, *Phys. Rev. A* **92**, 063610 (2015).
- [28] J. Zhang, S. Wu, Y. Zhang, and Z. Zhou, Generation of two-axis counter-twisting squeezed spin states via Uhrig dynamical decoupling, *Sci. China Inf. Sci.* **64**, 122502 (2021).
- [29] A. Z. Chaudhry and J. Gong, Protecting and enhancing spin squeezing via continuous dynamical decoupling, *Phys. Rev. A* **86**, 012311 (2012).
- [30] B. Yurke, S. L. McCall, and J. R. Klauder, SU(2) and SU(1,1) interferometers, *Phys. Rev. A* **33**, 4033 (1986).
- [31] T. Macrì, A. Smerzi, and L. Pezzè, Loschmidt echo for quantum metrology, *Phys. Rev. A* **94**, 010102(R) (2016).
- [32] E. Davis, G. Bentsen, and M. Schleier-Smith, Approaching the Heisenberg limit without single-particle detection, *Phys. Rev. Lett.* **116**, 053601 (2016).
- [33] F. Anders, L. Pezzè, A. Smerzi, and C. Klempt, Phase magnification by two-axis counter-twisting for detection-noise robust interferometry, *Phys. Rev. A* **97**, 043813 (2018).
- [34] D. Linnemann, H. Strobel, W. Muessel, J. Schulz, R. J. Lewis-Swan, K. V. Kheruntsyan, and M. K. Oberthaler, Quantum-enhanced sensing based on time reversal of nonlinear dynamics, *Phys. Rev. Lett.* **117**, 013001 (2016).
- [35] S. S. Mirkhalaf, S. P. Nolan, and S. A. Haine, Robustifying twist-and-turn entanglement with interaction-based readout, *Phys. Rev. A* **97**, 053618 (2018).
- [36] M. Gabbriellini, L. Pezzè, and A. Smerzi, Spin-mixing interferometry with Bose-Einstein condensates, *Phys. Rev. Lett.* **115**, 163002 (2015).
- [37] M. Manceau, G. Leuchs, F. Khalili, and M. Chekhova, Detection loss tolerant supersensitive phase measurement with an SU(1,1) interferometer, *Phys. Rev. Lett.* **119**, 223604 (2017).
- [38] J. Huang, M. Zhuang, and C. Lee, Non-Gaussian precision metrology via driving through quantum phase transitions, *Phys. Rev. A* **97**, 032116 (2018).
- [39] J. Huang, M. Zhuang, B. Lu, Y. Ke, and C. Lee, Achieving Heisenberg-limited metrology with spin cat states via interaction-based readout, *Phys. Rev. A* **98**, 012129 (2018).
- [40] S. A. Haine, Using interaction-based readouts to approach the ultimate limit of detection-noise robustness for quantum-enhanced metrology in collective spin systems, *Phys. Rev. A* **98**, 030303(R) (2018).
- [41] S. S. Szigeti, R. J. Lewis-Swan, and S. A. Haine, Pumped-up SU(1,1) interferometry, *Phys. Rev. Lett.* **118**, 150401 (2017).
- [42] M. Schulte, V. J. Martínez-Lahuerta, M. S. Scharnagl, and K. Hammerer, Ramsey interferometry with generalized one-axis twisting echoes, *Quantum* **4**, 268 (2020).
- [43] S. P. Nolan, S. S. Szigeti, and S. A. Haine, Optimal and robust quantum metrology using interaction-based readouts, *Phys. Rev. Lett.* **119**, 193601 (2017).
- [44] Q. Liu, T.-W. Mao, M. Xue, L.-N. Wu, and L. You, Cyclic nonlinear interferometry with entangled non-Gaussian spin states, *Phys. Rev. A* **107**, 052613 (2023).
- [45] F. Hudelist, J. Kong, C. Liu, J. Jing, Z. Ou, and W. Zhang, Quantum metrology with parametric amplifier-based

- photon correlation interferometers, *Nat. Commun.* **5**, 3049 (2014).
- [46] S. C. Burd, R. Srinivas, J. J. Bollinger, A. C. Wilson, D. J. Wineland, D. Leibfried, D. H. Slichter, and D. T. C. Allcock, Quantum amplification of mechanical oscillator motion, *Science* **364**, 1163 (2019).
- [47] O. Hosten, R. Krishnakumar, N. J. Engelsen, and M. A. Kasevich, Quantum phase magnification, *Science* **352**, 1552 (2016).
- [48] T.-W. Mao, Q. Liu, X.-W. Li, J.-H. Cao, F. Chen, W.-X. Xu, M. K. Tey, Y.-X. Huang, and L. You, Quantum-enhanced sensing by echoing spin-nematic squeezing in atomic Bose-Einstein condensate, *Nat. Phys.* **19**, 1585 (2023).
- [49] Z. Hu, Q. Li, X. Zhang, H.-B. Zhang, L.-G. Huang, and Y.-C. Liu, Nonlinear time-reversal interferometry with arbitrary quadratic collective-spin interaction, *Chin. Phys. B* **33**, 080601 (2024).
- [50] M. Zhuang, J. Huang, and C. Lee, Entanglement-enhanced test proposal for local Lorentz-symmetry violation via spinor atoms, *Quantum* **6**, 859 (2022).
- [51] F. Fröwis, P. Sekatski, and W. Dür, Detecting large quantum fisher information with finite measurement precision, *Phys. Rev. Lett.* **116**, 090801 (2016).
- [52] M. Zhuang, H. Huo, Y. Qiu, W. Liu, J. Huang, and C. Lee, Heisenberg-limited frequency estimation via driving through quantum phase transitions, *Phys. Rev. Appl.* **16**, 064056 (2021).
- [53] Z. Hu, Q. Li, X. Zhang, L.-G. Huang, H.-B. Zhang, and Y.-C. Liu, Spin squeezing with arbitrary quadratic collective-spin interactions, *Phys. Rev. A* **108**, 023722 (2023).
- [54] Q. Liu, L.-N. Wu, J.-H. Cao, T.-W. Mao, X.-W. Li, S.-F. Guo, M. K. Tey, and L. You, Nonlinear interferometry beyond classical limit enabled by cyclic dynamics, *Nat. Phys.* **18**, 167 (2022).
- [55] S. Colombo, E. Pedrozo-Peñañiel, A. F. Adiyatullin, Z. Li, E. Mendez, C. Shu, and V. Vuletić, Time-reversal-based quantum metrology with many-body entangled states, *Nat. Phys.* **18**, 925 (2022).
- [56] Z. Li, S. Colombo, C. Shu, G. Velez, S. Pilatowsky-Cameo, R. Schmied, S. Choi, M. Lukin, E. Pedrozo-Peñañiel, and V. Vuletić, Improving metrology with quantum scrambling, *Science* **380**, 1381 (2023).
- [57] C. Helstrom, Minimum mean-squared error of estimates in quantum statistics, *Phys. Lett. A* **25**, 101 (1967).
- [58] J. Huang, S. Wu, H. Zhong, and C. Lee, Quantum metrology with cold atoms, in *Annual Review of Cold Atoms and Molecules* (World Scientific, Singapore, 2014), Chap. 7, pp. 365–415.
- [59] R. Demkowicz-Dobrzański and L. Maccone, Using entanglement against noise in quantum metrology, *Phys. Rev. Lett.* **113**, 250801 (2014).
- [60] X. Long, W.-T. He, N.-N. Zhang, K. Tang, Z. Lin, H. Liu, X. Nie, G. Feng, J. Li, T. Xin, Q. Ai, and D. Lu, Entanglement-enhanced quantum metrology in colored noise by quantum Zeno effect, *Phys. Rev. Lett.* **129**, 070502 (2022).
- [61] X. Zhang, Z. Hu, and Y.-C. Liu, Fast generation of GHZ-like states using collective-spin XYZ model, *Phys. Rev. Lett.* **132**, 113402 (2024).
- [62] A. Datta, L. Zhang, N. Thomas-Peter, U. Dorner, B. J. Smith, and I. A. Walmsley, Quantum metrology with imperfect states and detectors, *Phys. Rev. A* **83**, 063836 (2011).